Referencing information

Quinn G. Reynolds. *Computational modelling of shear-layer instabilities and vortex formation in DC plasma arcs*, Minerals Engineering Journal - Special Edition: Proceedings of Computational Modelling 13 (2013), DOI 10.1016/j.mineng.2013.10.027

http://www.sciencedirect.com/science/article/pii/S0892687513003518

Computational modelling of shear-layer instabilities and vortex formation in DC plasma arcs

Q.G. Reynolds[a]
[a]*Corresponding Author. Pyrometallurgy Division, Mintek, Private Bag X3015, Randburg, 2125, South Africa. Email: quinnr@mintek.co.za. Ph: +27(0)117094416.*

Abstract

The direct-current plasma arc is the principal heating and stirring element in plasma arc furnaces. The arc is a highly dynamic system operating at very short time scales (milliseconds or less). This dynamic behavior can be understood as the combination of several modes of instability acting together. These modes can include fluid dynamic/shear layer instabilities, near-electrode instabilities resulting from steep local temperature gradients and other electrode surface effects, or helical/twisting instabilities resulting from the magnetic field generated in one part of the arc column exerting a force on another.

Computational magneto-hydrodynamic models of the arc which are able to reproduce the highly transient behavior of the system are developed to study certain dynamic modes – in particular, the formation and evolution of axisymmetric vortices and shear layer instabilities in the arc jet. Results from this work are then compared to qualitative data from high-speed photographic imaging of large plasma arcs (up to 3kA current).

Keywords: Pyrometallurgy, Computational Fluid Dynamics, Modelling

1. Introduction

Direct-current (DC) plasma arc furnaces have been used for metallurgical applications since 1878. For many years the scrap steel remelting industry was the largest consumer of the technology, however since the 1970s it has also begun to enter new primary-ore smelting markets with applications in commodities such as ferrochromium, ferronickel, and platinum group metals [Jones et al (2011)]. A diagram of the DC arc furnace showing the principal components is shown in Figure 1.

DC arc furnaces are typically operated in *open-arc* mode. This implies that the tip of the graphite electrode is always positioned above the surface of the molten bath, resulting in the formation of a plasma arc in the freeboard gas space between the tip and the bath. The plasma arc is the "engine room" of the DC arc furnace, providing mechanical and thermal energy input to the slag and metal baths at very high intensity.

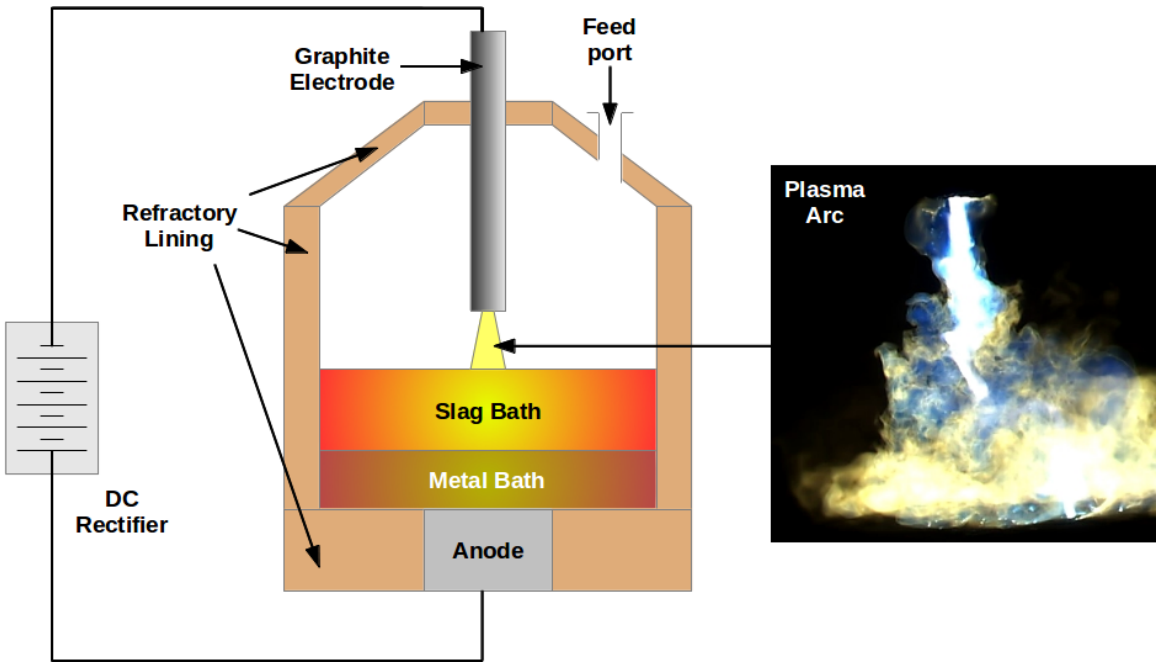

Figure 1: Schematic diagram of DC arc furnace

The arc itself consists of *plasma*, material in the fourth state of matter. Plasmas contain a mixture of neutral gas, positively charged ions, and free electrons, and result from the heating of gases to very high temperatures (> 6000K). Plasmas are electrically conductive, which enables the arc to complete the circuit between the electrode and the molten bath in the DC arc furnace. The plasma arc is a magneto-hydrodynamic (MHD) system – a high-velocity, high-temperature jet of conductive fluid sustained and driven by interactions between the various temperature, velocity, and electromagnetic fields.

At moderate to high current levels, the plasma arc is an inherently unstable, transient phenomenon and exhibits rapid motion and evolution over short time scales, of the order of milliseconds or less [Reynolds et al (2010)]. In the operation of DC arc furnaces, these rapid fluctuations can cause rectifier control problems (and even damage), arc extinction events, and other unwanted behaviour if they become too strong. As a result, it is highly desirable to gain an improved fundamental understanding of the instabilities that cause dynamic behaviour in arcs.

Arc instabilities may be classified into two broad categories: hydrodynamic and magnetic.

Hydrodynamic instabilities relate to fluid flow behaviour [Becker & Massaro (1968), Plaschko (1978)] in the arc jet and may include helical instabilities in which the arc column twists into a three-dimensional coil shape, and Kelvin-Helmholz instabilities resulting from the high shear gradient between the arc jet core and the surrounding fluid. The latter result in axisymmetric vortex disturbances forming around the arc column, and travelling along it while growing in size. Schematic diagrams showing the two modes of instability are shown in Figure 2(a) and (b).

Magnetic instabilities relate to the interaction of the arc with the electromagnetic fields in and around it [Lehnert (1967), Bowman (1994)]. By Ampere's law, the current density field ***j*** in the arc column produces a self-magnetic field ***B***. The Lorentz force, ***j*** x ***B***, can be very large and cause instability under certain conditions of arc geometry. Common examples include kink instabilities resulting from bends in the arc column being pushed outward by the local Lorentz force, and pinch instabilities (specifically z-pinch) caused by a constriction in the arc column – this results in a centripetal Lorentz force which acts to narrow the constriction further. Evolution of these instability types is shown schematically in Figures 2(c) and (d).

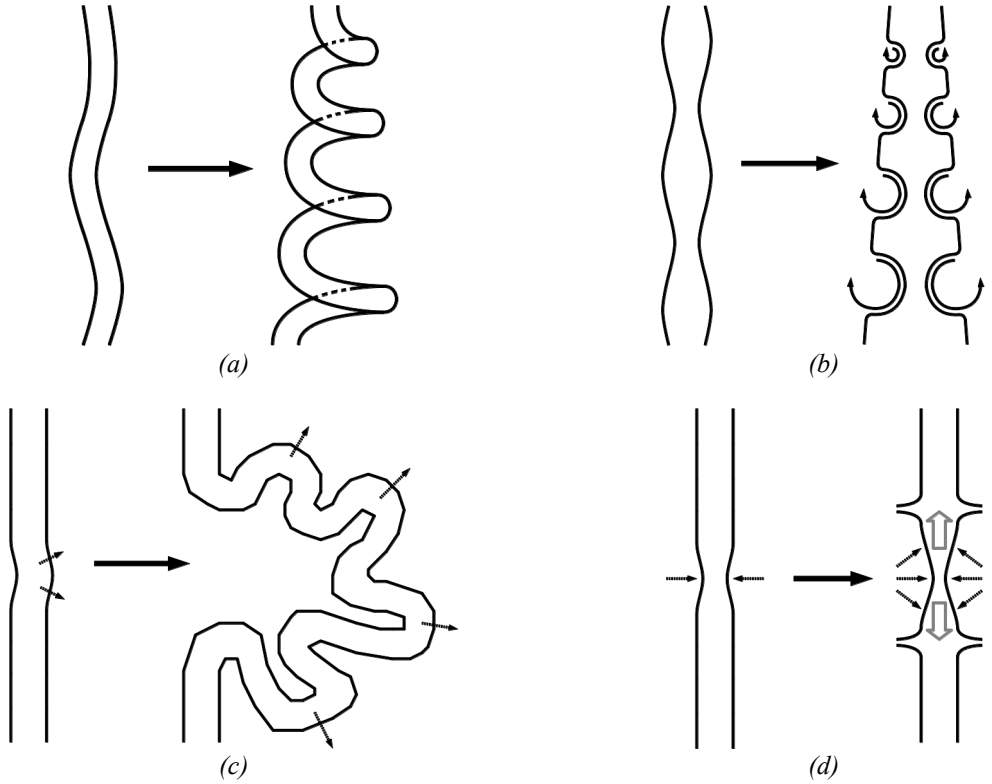

Figure 2: Diagrams of arc instability modes. (a) helical, (b) Kelvin-Helmholtz, (c) kink, (d) z-pinch

Some photographic examples of instability modes from various tests conducted at Mintek are shown in Figure 3. Unless otherwise indicated, all arcs were generated in ambient air between a graphite electrode and a flat graphite block connected as anode. A 3.2 MVA IGBT rectifier was used to provide DC current at between 1 and 3kA. The arcs were filmed using an Olympus iSpeed 3 high-speed digital video camera, at 5000 frames per second.

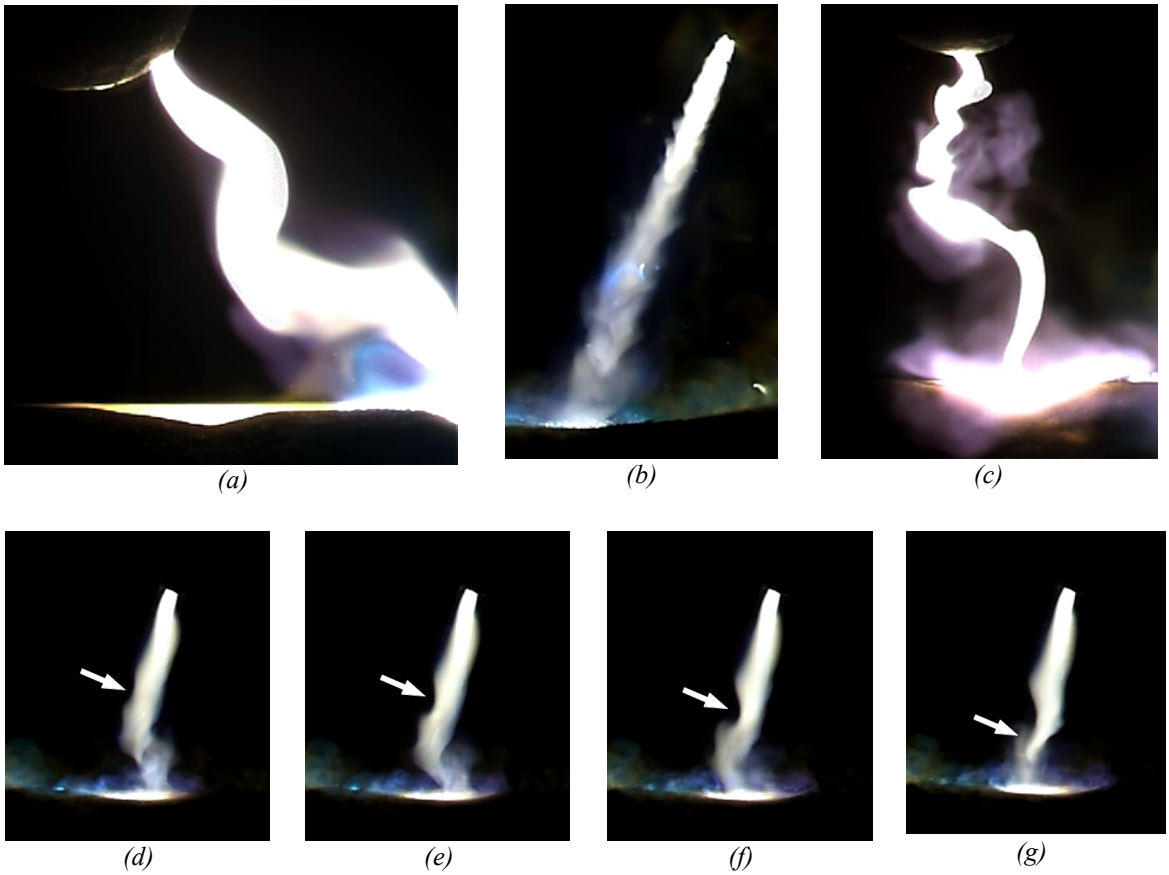

Figure 3: High speed photographs of instability modes in plasma arcs, (a) helical, (b) Kelvin-Helmholtz, (c) magnetic kink, (d)-(g) z-pinch formation (at arrow)

The plasma arc is generally operated in an enclosed space inside the freeboard of a DC furnace above a molten bath of process material, and interactions with this environment can be sources of additional instability. The gas in the vicinity of the arc frequently contains a heavy loading of fine particulate matter originating from either the feed material or fuming and recondensation of chemical components in the molten bath. This dust and fume can have several effects on the arc jet including cooling of the plasma, alteration of the plasma composition, and partial obstruction of the flow field by larger particles. These effects can exacerbate the onset of instabilities in the arc system by affecting either the physical properties of the plasma (which are functions of its composition and temperature) or the turbulence level of the flow.

Strong interaction between the arc jet and the molten bath is possible due to the high velocities in the arc, resulting in deformation and splashing at the surface of the molten material. Additionally, particles of unreacted raw material or reductant may float on the surface of the molten pool in the vicinity of the arc before they are consumed by reaction or melting. These effects both change the shape of the surface to which the arc attaches, and although occurring at a slower time scale (hundreds to thousands of milliseconds), may be an additional source of instability as the arc attempts to attach to the surface closest to the electrode.

The state of the art in mathematical and computational models of plasma arcs has advanced greatly over the past 30 years. The pioneering work of Szekely and co-workers [Ushio et al (1981)] first demonstrated the concept of applying computational fluid dynamics to the study of the arc, using simple fluid flow models and predetermined electromagnetic fields. More sophisticated models subsequently sought to include numerical solution of the electromagnetic component, full coupling of the fluid flow, temperature, and electromagnetic fields, complex plasma gas mixtures, and more [Szekely et al (1983), Gu et al (1993), Alexis (1999)]. A key feature of much of this work is the use of steady-state models, which while valuable from an engineering point of view are of limited applicability for evaluating arc instabilities.

Recent work has used three-dimensional dynamic MHD models to study the temporal evolution of arc systems [Reynolds et al (2010), Reynolds & Reddy (2011)]. While certain similarities between the models and observed phenomena were found, the behaviour of fully developed arcs was seen to be highly chaotic and complex. This suggests that many modes of instability may be operating simultaneously in both the models and real arcs. Development of a simplified two-dimensional dynamic model of the arc to study only the axisymmetric modes of instability in isolation was therefore deemed to be of some value.

2. Model description

The axisymmetric plasma arc model consists of three components – a fluid flow model, a heat transfer model, and an electromagnetic field model. The arc plasma is considered to be incompressible, optically thin, and in local thermodynamic equilibrium (LTE) [Boulos et al (1994)]. LTE allows the thermodynamic and transport properties of the fluid to be described as functions of temperature. A further approximation is made by treating the plasma density, viscosity, heat capacity and thermal conductivity as constant – as this work is primarily concerned with the qualitative dynamics of the system rather than absolute engineering accuracy, this is considered acceptable. The strong, non-linear dependence of electrical conductivity and energy loss by radiation on temperature is retained in the model, providing additional coupling interactions.

The Navier-Stokes and continuity equations in cylindrical coordinates describe the velocity distribution for fluid flow problems. For the plasma arc model, source terms for the Lorentz force must be included. This gives:

$$\frac{\partial v_r}{\partial t} + v_r \frac{\partial v_r}{\partial r} + v_z \frac{\partial v_r}{\partial z} + \frac{1}{\rho}\frac{\partial P}{\partial r} = \frac{\mu}{\rho}\left[\frac{\partial}{\partial r}\left(\frac{1}{r}\frac{\partial}{\partial r}(r v_r)\right) + \frac{\partial^2 v_r}{\partial z^2}\right] - \frac{j_z B_\theta}{\rho} \tag{1a}$$

$$\frac{\partial v_z}{\partial t} + v_r \frac{\partial v_z}{\partial r} + v_z \frac{\partial v_z}{\partial z} + \frac{1}{\rho}\frac{\partial P}{\partial z} = \frac{\mu}{\rho}\left[\frac{1}{r}\frac{\partial}{\partial r}\left(r\frac{\partial v_z}{\partial r}\right) + \frac{\partial^2 v_z}{\partial z^2}\right] + \frac{j_r B_\theta}{\rho} \tag{1b}$$

$$\frac{1}{r}\frac{\partial}{\partial r}(r v_r) + \frac{\partial v_z}{\partial z} = 0 \tag{1c}$$

Here, v_r and v_z are the radial and azimuthal components of the velocity vector, ρ is the fluid density, and μ is its viscosity. j_r and j_z are the radial and azimuthal components of the current density vector, and B_θ is the magnitude of the magnetic field vector (perpendicular to the current vector).

The energy equation describes heat transfer in the arc system:

$$\frac{\partial T}{\partial t} + v_r \frac{\partial T}{\partial r} + v_z \frac{\partial T}{\partial z} = \frac{\kappa}{\rho C_P}\left[\frac{1}{r}\frac{\partial}{\partial r}\left(r\frac{\partial T}{\partial r}\right) + \frac{\partial^2 T}{\partial z^2}\right] + \frac{1}{\rho C_P}\left(\frac{j_r^2 + j_z^2}{\sigma} - Q_R\right) \quad (2)$$

Here, T is the plasma temperature, κ is the plasma thermal conductivity, C_P is its heat capacity, and σ is its electrical conductivity. The source term describes energy generation by Ohmic heating, and energy loss by radiation. Both σ and Q_R are functions of temperature.

Finally, the current conservation law and Ampere's law are used to describe the electromagnetic fields:

$$\frac{1}{r}\frac{\partial}{\partial r}\left(r\sigma\frac{\partial \phi}{\partial r}\right) + \frac{\partial}{\partial z}\left(\sigma\frac{\partial \phi}{\partial z}\right) = 0 \quad (3a)$$

$$j_r = -\sigma\frac{\partial \phi}{\partial r}, j_z = -\sigma\frac{\partial \phi}{\partial z} \quad (3b)$$

$$\frac{1}{r}\frac{\partial}{\partial r}(rB_\theta) = \mu_0 j_z \quad (3c)$$

Here, ϕ is the electric potential field and μ_0 is a physical constant, the permeability of free space.

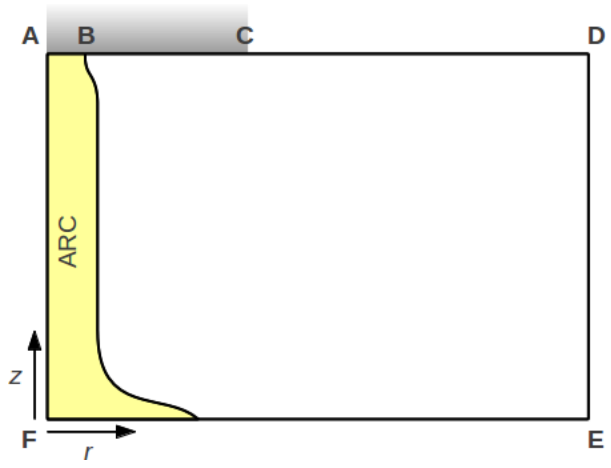

Figure 4: Diagram showing geometry of model region

The region modelled is shown in Figure 4. In this diagram, F is the origin of an axisymmetric coordinate system. AF is the centerline of the arc and electrode. AB is the arc attachment zone, in which current is supplied from the electrode tip to the arc plasma by thermionic emission. The current density in this zone is taken as a constant, j_k = 3.5 kA/cm^2 [Bowman (1994)], which allows determination of the zone size r_{AB} from the specified total current. ABC is the surface of the graphite electrode tip. CDE is treated as a solid wall for the purposes of the model. EF is the surface of the molten bath. Due to the very short time scales modelled in the plasma arc, this surface is also treated as solid. Boundary conditions for the various fields are shown in Table 1.

Table 1: Boundary conditions for axisymmetric arc model

	AB	BC	CD
$\boldsymbol{v}$	$v_r = v_z = 0$	$v_r = v_z = 0$	$v_r = v_z = 0$
T	$-\kappa\frac{\partial T}{\partial z} = h_E(T - T_E)$	$-\kappa\frac{\partial T}{\partial z} = h_E(T - T_E)$	$-\kappa\frac{\partial T}{\partial z} = h_W(T - T_W)$
ϕ	$-\sigma\frac{\partial \phi}{\partial z} = j_k$	$\frac{\partial \phi}{\partial z} = 0$	$\frac{\partial \phi}{\partial z} = 0$
B_θ	-	-	-
	DE	EF	AF
$\boldsymbol{v}$	$v_r = v_z = 0$	$v_r = v_z = 0$	$v_r = \frac{\partial v_z}{\partial z} = 0$
T	$-\kappa\frac{\partial T}{\partial r} = h_W(T - T_W)$	$-\kappa\frac{\partial T}{\partial z} = h_A(T - T_A)$	$\frac{\partial T}{\partial r} = 0$
ϕ	$\frac{\partial \phi}{\partial r} = 0$	$\phi = 0$	$\frac{\partial \phi}{\partial r} = 0$
B_θ	-	-	$B_\theta = 0$

Here, h_E and T_E are the heat transfer coefficient at the surface of the electrode and the temperature of the electrode respectively. Similarly, h_A and T_A pertain to the anode surface, and h_W and T_W to the boundary walls. In all cases modelled here, very high values of the h_i are used in order to approximate constant-temperature boundary conditions.

The time-dependent fluid flow and energy equations are solved using a second-order finite difference discretization for the spatial variables, and an explicit forward time-stepping technique using operator splitting combined with a fourth-order Runge-Kutta method. Elliptic equations arising as a result of the pressure variable in the Navier-Stokes equation as well as the electric potential equation (3a) require solution at each time-step or Runge-Kutta stage, and are solved using a geometric multigrid approach. The overall method is designed to be as simple as possible while retaining acceptable accuracy, in order to scale to very high spatial and temporal resolutions – as no turbulence closure models are used, all spatial resolutions down to the viscous level are modelled directly.

For this study, the models were written in ANSI C and compiled using GCC 4.6.3. OpenMP directives were used for loop parallelisation to enhance performance on symmetric multiprocessor architectures. Typical run times varied from 2 to 3 hours on quad-core systems using Intel Q6600 CPUs.

Further detail concerning the mathematical and numerical models used to study the plasma arc problem (in particular the three-dimensional models) may be found in other publications [Reynolds & Reddy (2011)].

3. Results and discussion

To study the plasma arc behaviour in the axisymmetric model, a base case was identified for a 5cm arc at 0.5kA in an air atmosphere. For the constant physical property values, averages between 5000K and 20000K were used [Boulos et al (1994)]. The parameters of the base case model are shown in Table 2.

The initial conditions are taken as "flash start" values, uniform temperature of 10000K and a uniform velocity of zero. This permits the arc jet to start up naturally through a flash of stagnant plasma between the electrode and anode surfaces.

Table 2: Base case axisymmetric arc model parameters

Parameter	*Value*	*Parameter*	*Value*
r_{AD} (region diameter)	0.1 m	μ	1.307×10^{-4} Pa.s
z_{AF} (region height)	0.05 m	ρ	0.02593 kg/m^3
r_{AC} (electrode diameter)	0.025 m	κ	3.067 W/m.K
Arc current	500 A	C_P	9420 J/kg.K
j_k	3.5×10^7 A/m^2	T_E	4100 K
Simulation time	100 ms	T_W	2000 K
Mesh resolution	513 x 257	T_A	3000 K

3.1 Base case - initial behaviour

A steady arc jet directed away from the electrode toward the anode forms initially, forming the classical bell-shaped profile associated with plasma arcs. From 2ms however, a strong recirculation pattern develops in the vicinity of the arc attachment zone on the electrode, and a ring vortex is shed from the high-shear region near the root of the arc. This disturbance is accelerated down the arc column by entrainment in the jet flow, growing larger and weaker until it reaches the anode at which point it is deflected into the stagnant fluid surrounding the arc jet and dissipates. This pattern repeats several times until the arc settles into a pseudo-steady state. Plots of the temperature field at various times during the first few milliseconds of arc evolution are shown in Figure 5.

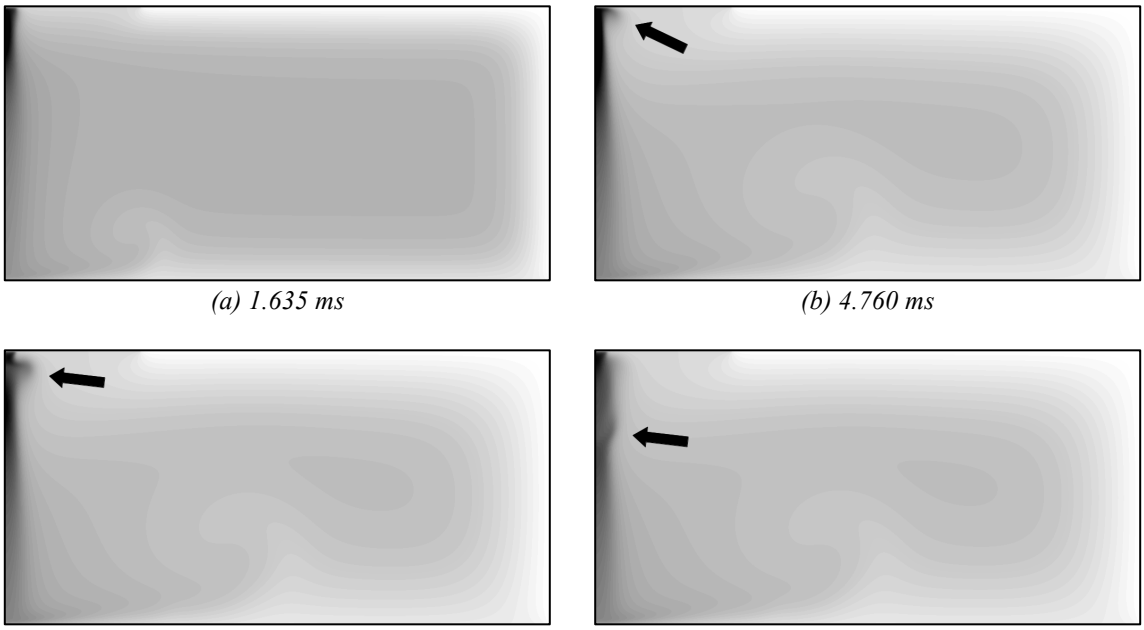

(a) 1.635 ms *(b) 4.760 ms*

(c) 5.142 ms *(d) 5.251 ms*

Figure 5: Temperature field plots – scale 2000K (white) to 15000K (black), (a) initial steady jet, (b)-(d) ring vortex formation and transport at arrow

The oscillating pattern of vortex shedding is clearly visible in the velocity and temperature values on the arc centerline, mid-way between the electrode and the anode – this is shown in Figure 6. The period of the vortex shedding behaviour rises as the simulation proceeds and the arc settles toward a pseudo-steady state.

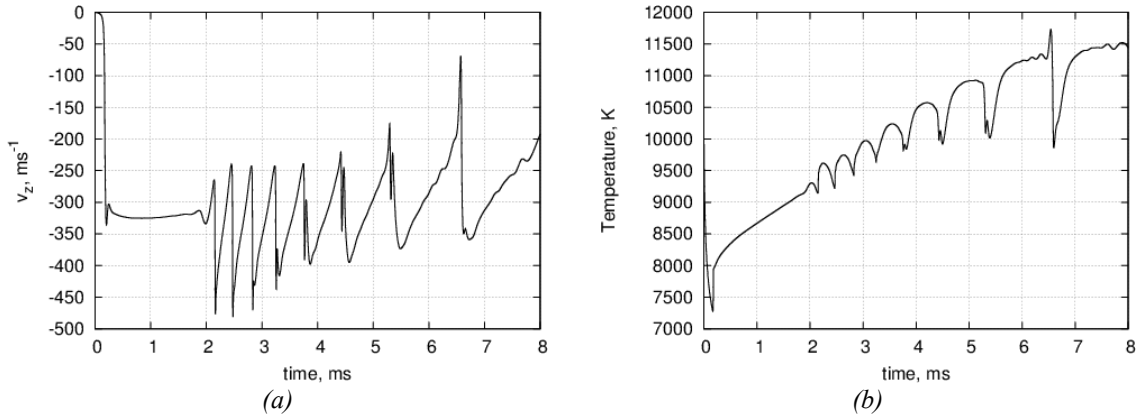

(a) *(b)*

Figure 6: Plots of (a) v_z component of velocity and (b) temperature as functions of time at z=25mm on arc centerline

3.2 Base case - transition behaviour in fully-developed flow

After the decay of the initial conditions and early behaviour, the plasma arc model is seen to operate in a mode of *punctuated equilibrium*; periods of steady, pseudo-stable arc operation are interspersed with highly-variable transient behaviour. This is qualitatively

similar to the rapid transitions between stable and unstable conditions frequently observed in real arcs [Reynolds (2012)].

Evidence of the transitions between pseudo-steady and transient behaviour can be seen in the variation of velocity and temperature at the midpoint of the arc centerline over the duration of the simulation, as shown in Figure 7.

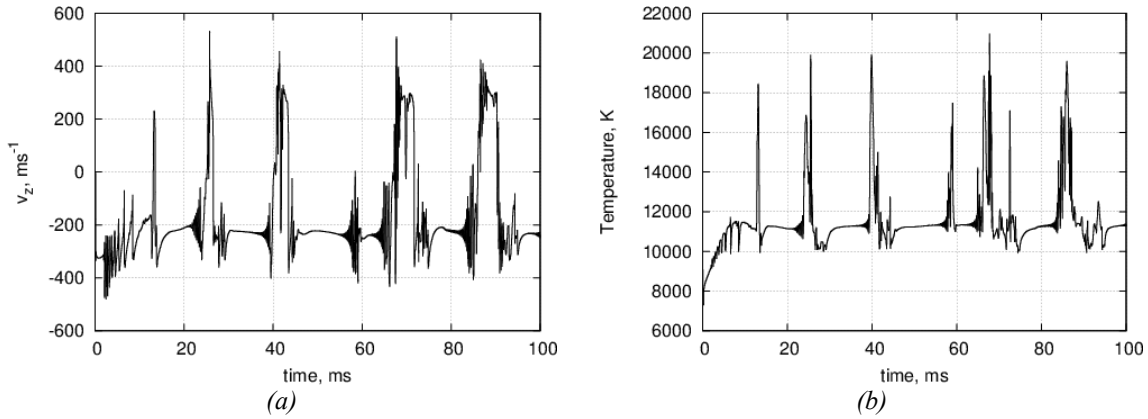

Figure 7: Graphs showing (a) v_z component of velocity and (b) temperature as functions of time at z=25mm on arc centerline

The unstable-regime events all have a similar morphology (see example in Figure 8). Starting from a pseudo-steady state, the transition event begins with the appearance of small regular oscillations in the fields. These grow rapidly in amplitude for about 2 ms, after which a breakdown into more chaotic, unpredictable behaviour occurs. This chaotic motion persists for an additional 7 to 10 ms, after which the arc system returns to the pseudo-steady state condition.

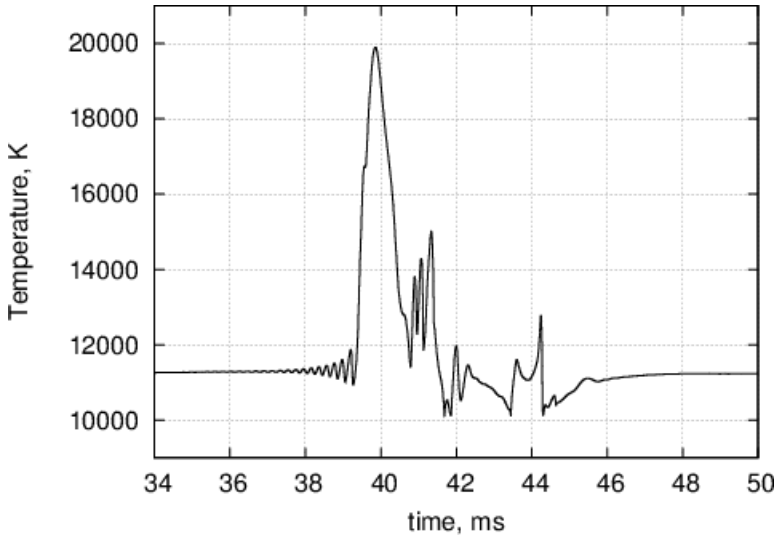

Figure 8: Behaviour of temperature with time during a single transition event (arc centerline, z=25mm)

In order to understand the exact process of transition into dynamic behaviour, it is helpful to examine the spatial structure of the plasma arc model at various points during the transition event shown in Figure 8. These are presented in the form of temperature field plots in Figure 9.

The transition event is initiated by a fluid dynamic instability – the pseudo-steady arc column begins to oscillate as the steep shear gradient between the core of the arc jet and the surrounding fluid breaks down in a Kelvin-Helmholtz instability. This results in axisymmetric rippling and vortex formation around the arc column, as seen in Figure 9a. Shortly after this behaviour commences the oscillations become large enough to cause significant constriction of the arc column, at which point a magnetic instability mode is triggered – a z-pinch instability can be seen forming near the center of the arc in Figure 9b. Strong plasma jets are ejected from above and below the z-pinch due to the magnetic compression, and interact violently with the established arc jet flow. This results in chaotic flow patterns and partial stalling of the arc jet, which permits a temporary anode arc to form (Figure 9c), and eventually leads to reestablishment of the pseudo-steady condition (Figure 9d).

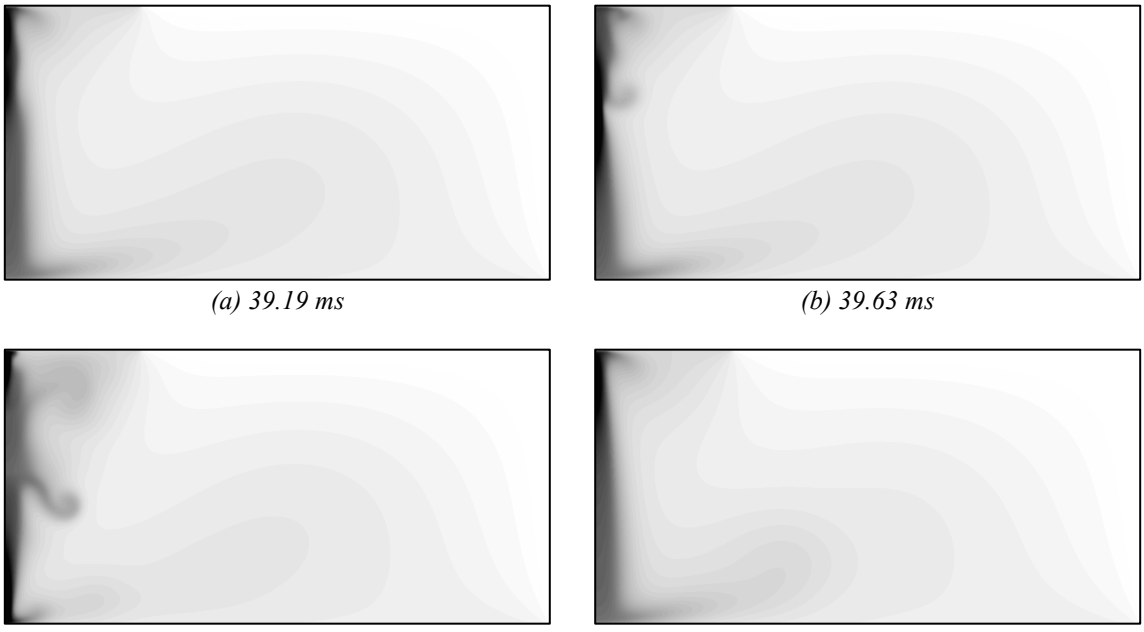

(a) 39.19 ms *(b) 39.63 ms*

(c) 41.92 ms *(d) 47.89 ms*

Figure 9: Temperature field plots at various times during transition event – scale 2000K (white) to 15000K (black)

The mechanism of fluid-dynamic instabilities initiating transient behaviour and later triggering magnetic instabilities has also been observed in real arcs. Figure 10 shows high-speed photography of a 3kA arc in air breaking down from a pseudo-stable jet into kink and z-pinch instabilities via a helical instability transition.

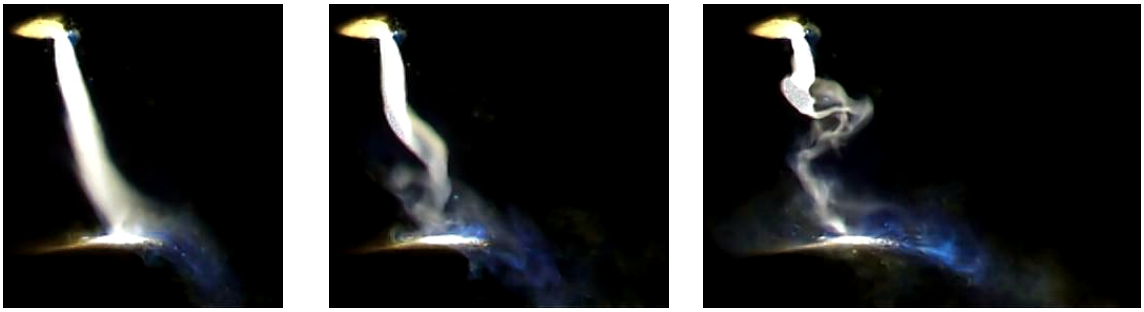

(a) 407.2 ms *(b) 428.2 ms* *(c) 452.4 ms*

Figure 10: High-speed photography sequence, (a) pseudo-steady arc, (b) onset of helical instability, (c) triggering of magnetic kink and z-pinch instabilities

3.3 Base case – heat transfer behaviour

The total thermal energy transferred by convection to the anode and cathode surfaces is calculated at each time step in the plasma arc model. The results are shown in Figure 11.

It is interesting to observe that the two boundaries behave very differently. At the electrode tip (cathode), the onset of transient behaviour produces very erratic heat transfer as might be expected, and generally *increases* the total energy transferred to the electrode. On the other hand, periods of transient behaviour act to *reduce* the energy transferred to the molten bath surface. This is initially somewhat counter-intuitive, since the overall turbulence of the flow is increased during these periods and one would expect the heat transfer at all surfaces to increase accordingly.

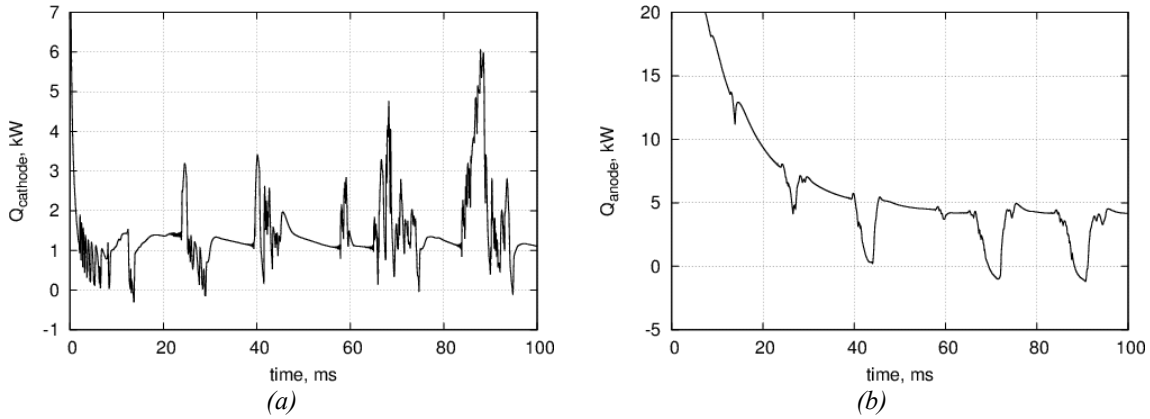

(a) *(b)*

Figure 11: Convective heat transfer rates to (a) electrode tip and (b) molten bath surface

A possible explanation is that the disappearance of the strong, steady arc jet blowing down onto the bath surface reduces the heat transfer rate at this surface during these events. Similarly, during z-pinch instability events, strong plasma jets are often observed directed back up the arc column toward the electrode tip; this "blowback" effect is also seen in experimental work and may be a contributing factor to the increased heat transfer experienced at the cathode (see Figure 12).

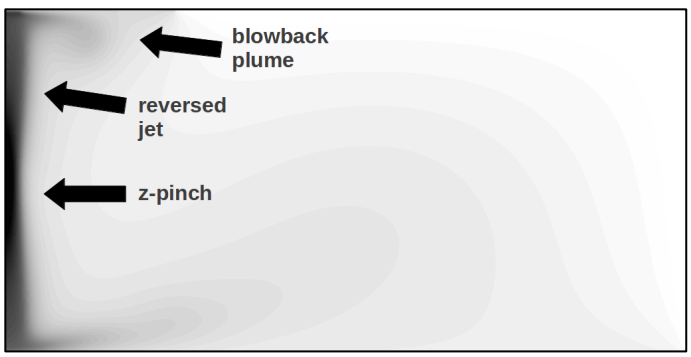

(a) 40.20 ms

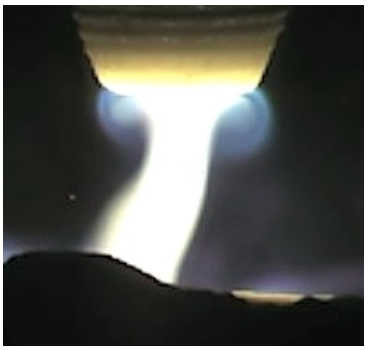

(b)

Figure 12: (a) Temperature field plot from plasma arc model showing arc jet reversal and blowback onto electrode surface, (b) high-speed photography of blowback plume on 2kA arc

Increased heat transfer to the electrode surface would result in higher graphite erosion rates, and lowered heat transfer to the molten bath would reduce the amount of energy available for melting and smelting reactions.

Instabilities in the plasma arc therefore have a direct bearing on the interaction between the arc and the raw materials fed to the furnace. The arc transfers the bulk of its thermal energy and momentum into the molten bath via convection – instabilities, particularly of the three-dimensional variety, can cause this transfer to be spread over a much larger area than if the arc was operating as a steady jet. Stalling and partial reversal of the jet flow in the arc also appear to be more likely when instabilities are present, further reducing the heat transfer to the bath and process material.

It may be concluded that stable arcs are more desirable in terms of the operation of DC arc furnaces, however in practice it is very difficult to control the arc stability at high power.

3.4 Effect of arc current on model behaviour

Previous work [Reynolds et al (2010)] has indicated that the arc's motion becomes progressively more chaotic and unstable in nature as the current is raised, in both models and the real world. This is understandable as the driving force acting on the plasma fluid, the Lorentz $\boldsymbol{j}$ x $\boldsymbol{B}$ source term, scales approximately with the square of the applied current.

The sensitivity of the axisymmetric plasma arc model to current displays similar tendencies. Variation of the arc voltage with time is shown in Figure 13, comparing results for arcs at 250A and 750A. An image of the temperature field from the model at 750A current is also shown.

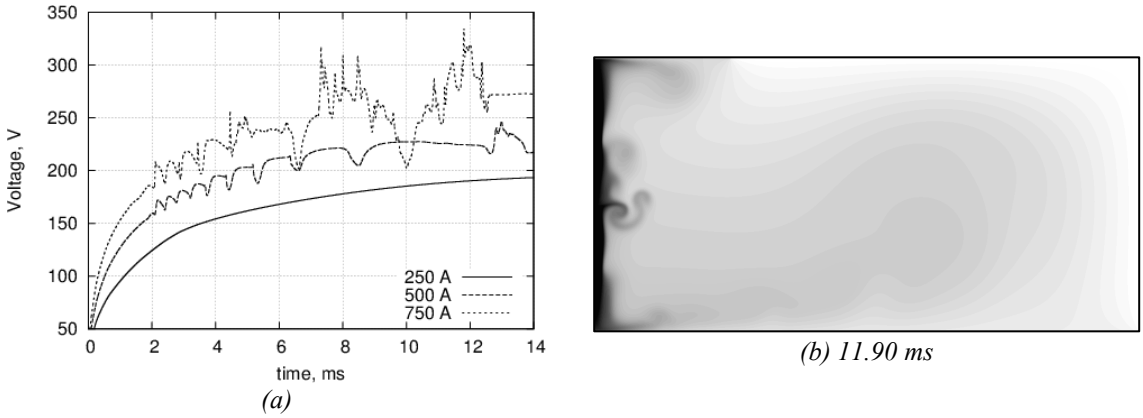

(a)

(b) 11.90 ms

Figure 13: (a) Arc voltage behaviour at different currents, (b) temperature field plot for arc at 750A showing turbulent flow around arc column – scale 2000K (white) to 15000K (black)

It can be seen that when operated at 250A, the arc model develops to a fixed steady state with little or no variation in time. This is in contrast to the punctuated equilibrium at 500A, and the unstable and highly chaotic motion at 750A. Increasing current in the axisymmetric arc model results in an increase in the time the arc system spends in unstable modes of operation.

3.5 Effect of plasma gas on model behaviour

Plasma arcs using air as the plasma gas are convenient for experimental study, but are somewhat atypical in welding and furnace applications. Generally the arc operates in a mixture of gases generated by the process (CO, Si, Fe, etc), or an artificially-introduced inert gas.

Table 3: Argon case model parameters

Parameter	*Value*	*Parameter*	*Value*
μ	1.408 x 10^{-4} Pa.s	κ	1.665 W/m.K
ρ	0.04898 kg/m^3	C_P	3715 J/kg.K

With this in mind, the axisymmetric plasma arc model was run using data for Argon [Boulos et al (1994)] for comparison purposes. Parameters for the model were identical to those given in Table 2, with the exception of the values shown in Table 3. Temperature-dependent values of σ and Q_R appropriate for Argon plasmas were also used.

The variation of arc voltage with time for the two plasma gases is shown in Figure 14, along with an indicative temperature field plot of the Argon arc.

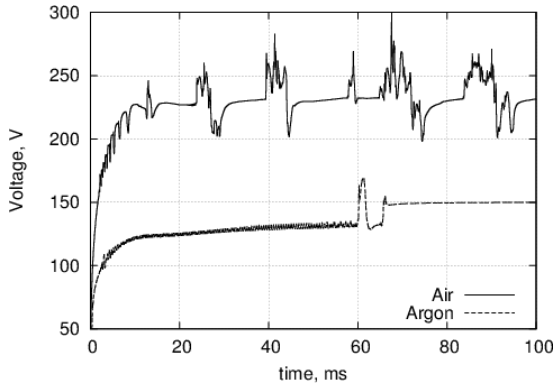

(a)

(b) 45.65 ms

Figure 14: (a) Variation of arc voltage with time for different plasma gases, (b) Temperature field plot for Argon model – scale 2000K (white) to 15000K (black)

The Argon system operates at lower voltage due to the development of a physically wider arc column, resulting in reduced current density in the main body of the arc. The lowered current density may also cause the observed reduction in unstable behaviour, in particular the triggering of magnetic instabilities by fluid-dynamic instabilities. The long period of regular oscillations seen up to 50 ms in the Argon system is indicative of the presence of shear layer instabilities, however these only trigger a single magnetic instability event during the 100ms simulation time compared to several in the air system.

3.6 Comparison with three-dimensional models

It is instructive to compare the results of the axisymmetric dynamic arc model with data generated by three-dimensional (3D) models. The latter are able to reproduce the full range of instabilities common to plasma arcs, including the asymmetric modes. Unfortunately the computational expense associated with running high-resolution 3D models is still prohibitively high, however the situation is improving constantly with the continued growth in available computer power.

For this test, a single 500A arc in a rectangular box 0.1 x 0.1 x 0.05m in dimensions was modelled on a mesh of 513 x 513 x 257 resolution. All arc model parameters were kept the same as those shown in Table 2, with the exception of the extension to three dimensions and a shorter simulation time (5 ms) necessitated by hardware limitations. Details of the mathematical and numerical formulation for the 3D plasma arc model may be found elsewhere [Reynolds & Reddy (2011)].

Figure 15 shows the evolution of the temperature field in both models at the midpoint of the arc centerline. Both models predict similar behaviour until approximately 0.8 ms, at which point a helical instability appears in the 3D model and disrupts the arc column (Figure 16a). This develops rapidly into a highly chaotic dynamic state, in which the arc column exhibits evidence of both hydrodynamic and magnetic instabilities (Figure 16b). The motion is qualitatively reminiscent of photographic evidence of dynamic arc behaviour.

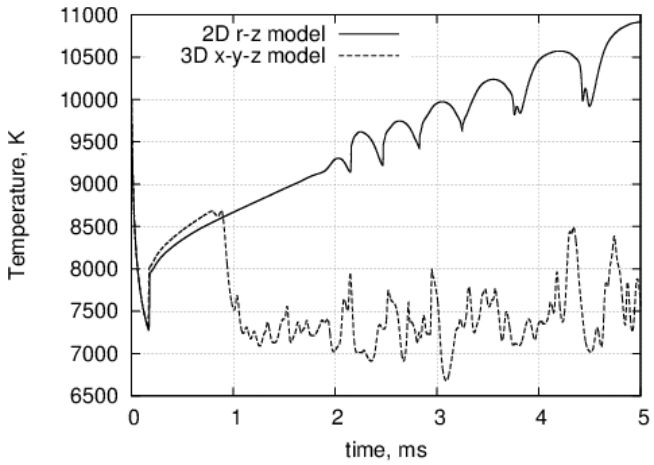

Figure 15: Temperature trends in 2D and 3D models on arc centerline, z = 25mm

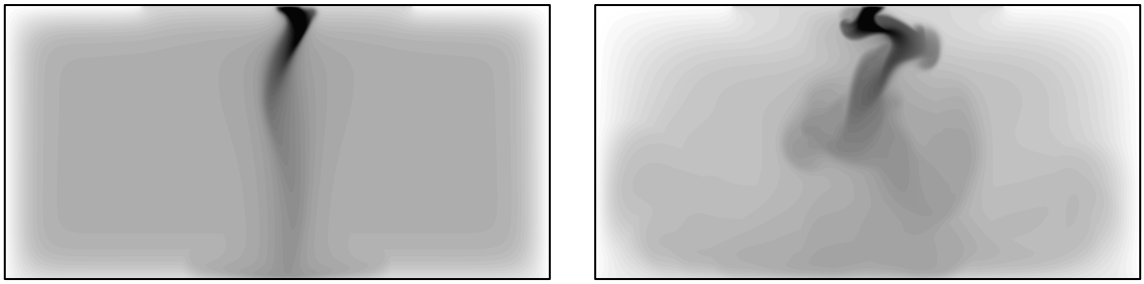

(a) 0.917 ms *(b) 4.715 ms*

Figure 16: XZ-projections of temperature field from 3D model – scale 2000K (white) to 15000K (black), (a) onset of helical instability, (b) "typical" chaotic motion with multimodal instability

It would appear that the simultaneous action of many instability modes, symmetric and asymmetric, contribute to the highly dynamic motion experienced in both 3D plasma arc models and real arcs.

4. Conclusions

Development of a dynamic computational model of DC plasma arcs using an axisymmetric formulation was successful, and complements existing two- and three-dimensional arc modelling work. By enforcing rotational symmetry, it was possible to isolate and study certain hydrodynamic and magnetic instability modes that contribute to the very complex, chaotic dynamics of real arcs.

It was observed that hydrodynamic shear-layer instabilities tend to initiate transitions between pseudo-steady and dynamic arc behaviour. Growth of the hydrodynamic instabilities was seen to trigger magnetic instabilities such as z-pinch constriction, with the combination of modes resulting in erratic and turbulent flow patterns in the arc.

Dynamic heat transfer to the molten bath and graphite electrode in the model was evaluated. It was found that the evolution of strong magnetic instabilities in the arc

column resulted in increased heat transfer to the electrode, and reduced heat transfer to the bath.

Sensitivity of the model to the arc current and plasma generating gas composition was briefly examined, and supported previous work suggesting that the nature of the arc dynamics is to some degree dependent on the model parameters used.

Finally, comparison of results from the 2D axisymmetric model with data from a 3D plasma arc model demonstrated how the many different symmetric and asymmetric plasma instability modes available in three dimensions can lead to more realistic, chaotic arc dynamics. A similar mechanism of instability-triggering – hydrodynamic first, then magnetic – was observed in the 3D model.

Further study and refinement of the axisymmetric plasma arc model is warranted. In particular, extension of both 2D and 3D models to incorporate more realistic plasma fluid descriptions (variable physical properties, two-temperature plasmas) would be of value. Inclusion of multiphase flow and/or a more generalized geometry at the anode surface to represent effects of the deformation of the molten bath would also be desirable. Correlative comparison between temporal data from the 2D and 3D models, and experimental measurements if possible, would be of interest in evaluating whether the individual contributions of various plasma instability modes could be practically identified from such information.

5. Acknowledgements

This paper is published by permission of Mintek. The author gratefully acknowledges the CSIR/Meraka Institute Centre for High Performance Computing, who provided access to their facilities in order to run the larger computational models.

6. References

Jones, R.T., Reynolds, Q.G., Curr, T.R. and Sager, D., Some myths about DC furnaces. In *Proc. Southern African Pyrometallurgy 2011*. Southern African Institute of Mining and Metallurgy (SAIMM), Johannesburg, 2011, pp 15 – 32

Plaschko, P., Helical instabilities of slowly diverging jets. Journal of Fluid Mechanics, 1979, 92 (2), pp 209 – 215

Becker, H.A. and Massaro, T.A., Vortex evolution in a round jet. Journal of Fluid Mechanics, 1968, 31 (3), pp 435 – 448

Lehnert, B., Experimental Evidence of Plasma Instabilities. Plasma Physics, 1967, 9, pp 301 – 337

Bowman, B., Properties of Arcs in DC Furnaces. In *Proc. 52nd Electric Furnace Conference*. Iron and Steel Society (ISS), Nashville, 1994, pp 111-120

Ushio, M., Szekely, J. and Chang, C.W., Mathematical modelling of flow field and heat transfer in high-current arc discharge. Ironmaking and Steelmaking, 1981, 8 (6), pp 279 – 286

Szekely, J., Mckelliget, J. and Choudhary, M., Heat-transfer fluid flow and bath circulation in electric arc furnaces and DC plasma furnaces. Ironmaking and Steelmaking, 1983, 10 (4), pp 169 – 179

Gu, L., Jensen, R. and Bakken, J.A., Metal vapour infiltration in Argon arcs used for heating liquid metal. In *Proc. 51st Electric Furnace Conference*. Iron and Steel Society (ISS), Washington DC, 1993, pp 193 – 199

Alexis, J., Ramirez, M. and Trapaga, G., Modeling of heat transfer from an electric arc – a simulation of heating Part I. In *Proc. 57th Electric Furnace Conference*. Iron and Steel Society (ISS), Pittsburg, 1999, pp 279 – 287

Reynolds, Q.G., Jones, R.T. and Reddy, B.D., Mathematical and computational modelling of the dynamic behaviour of direct current plasma arcs. In *Proc. 12th International Ferro-Alloys Congress*. Outotec Oyj, Helsinki, 2010, pp 789 – 801

Reynolds, Q.G. and Reddy, B.D., Some aspects of dynamic computational modelling of direct current plasma arc phenomena. In *Proc. 4th International Conference on Computational Methods for Coupled Problems in Science and Engineering*. International Centre for Numerical Methods in Engineering (CIMNE), Kos, 2011, pp 1239 – 1250

Reynolds, Q.G., Plasma Arc Extinction Events - Insights from High-Speed Photography and Modelling. In *Proc. 30th International Congress on High Speed Imaging and Photonics*. Scientific Committee of the 30th International Congress on High Speed Imaging and Photonics (ICHSIP30), Pretoria, 2012, pp 67 – 73

Boulos, M.I., Fauchais, P. and Pfender, E., *Thermal Plasmas Volume 1 – Fundamentals and Applications*, 1994, Plenum Press, New York